FERMILAB-PUB-09-092-E

Combination and interpretations of $t\bar{t}$ cross section measurements with the D0 detector

V.M. Abazov[37], B. Abbott[75], M. Abolins[65], B.S. Acharya[30], M. Adams[51], T. Adams[49], E. Aguilo[6], M. Ahsan[59], G.D. Alexeev[37], G. Alkhazov[41], A. Alton[64,a], G. Alverson[63], G.A. Alves[2], L.S. Ancu[36], T. Andeen[53], M.S. Anzelc[53], M. Aoki[50], Y. Arnoud[14], M. Arov[60], M. Arthaud[18], A. Askew[49,b], B. Åsman[42], O. Atramentov[49,b], C. Avila[8], J. BackusMayes[82], F. Badaud[13], L. Bagby[50], B. Baldin[50], D.V. Bandurin[59], S. Banerjee[30], E. Barberis[63], A.-F. Barfuss[15], P. Bargassa[80], P. Baringer[58], J. Barreto[2], J.F. Bartlett[50], U. Bassler[18], D. Bauer[44], S. Beale[6], A. Bean[58], M. Begalli[3], M. Begel[73], C. Belanger-Champagne[42], L. Bellantoni[50], A. Bellavance[50], J.A. Benitez[65], S.B. Beri[28], G. Bernardi[17], R. Bernhard[23], I. Bertram[43], M. Besançon[18], R. Beuselinck[44], V.A. Bezzubov[40], P.C. Bhat[50], V. Bhatnagar[28], G. Blazey[52], S. Blessing[49], K. Bloom[67], A. Boehnlein[50], D. Boline[62], T.A. Bolton[59], E.E. Boos[39], G. Borissov[43], T. Bose[62], A. Brandt[78], R. Brock[65], G. Brooijmans[70], A. Bross[50], D. Brown[19], X.B. Bu[7], D. Buchholz[53], M. Buehler[81], V. Buescher[22], V. Bunichev[39], S. Burdin[43,c], T.H. Burnett[82], C.P. Buszello[44], P. Calfayan[26], B. Calpas[15], S. Calvet[16], J. Cammin[71], M.A. Carrasco-Lizarraga[34], E. Carrera[49], W. Carvalho[3], B.C.K. Casey[50], H. Castilla-Valdez[34], S. Chakrabarti[72], D. Chakraborty[52], K.M. Chan[55], A. Chandra[48], E. Cheu[46], D.K. Cho[62], S. Choi[33], B. Choudhary[29], T. Christoudias[44], S. Cihangir[50], D. Claes[67], J. Clutter[58], M. Cooke[50], W.E. Cooper[50], M. Corcoran[80], F. Couderc[18], M.-C. Cousinou[15], S. Crépé-Renaudin[14], V. Cuplov[59], D. Cutts[77], M. Ćwiok[31], A. Das[46], G. Davies[44], K. De[78], S.J. de Jong[36], E. De La Cruz-Burelo[34], K. DeVaughan[67], F. Déliot[18], M. Demarteau[50], R. Demina[71], D. Denisov[50], S.P. Denisov[40], S. Desai[50], H.T. Diehl[50], M. Diesburg[50], A. Dominguez[67], T. Dorland[82], A. Dubey[29], L.V. Dudko[39], L. Duflot[16], D. Duggan[49], A. Duperrin[15], S. Dutt[28], A. Dyshkant[52], M. Eads[67], D. Edmunds[65], J. Ellison[48], V.D. Elvira[50], Y. Enari[77], S. Eno[61], P. Ermolov[39,‡], M. Escalier[15], H. Evans[54], A. Evdokimov[73], V.N. Evdokimov[40], G. Facini[63], A.V. Ferapontov[59], T. Ferbel[61,71], F. Fiedler[25], F. Filthaut[36], W. Fisher[50], H.E. Fisk[50], M. Fortner[52], H. Fox[43], S. Fu[50], S. Fuess[50], T. Gadfort[70], C.F. Galea[36], A. Garcia-Bellido[71], V. Gavrilov[38], P. Gay[13], W. Geist[19], W. Geng[15,65], C.E. Gerber[51], Y. Gershtein[49,b], D. Gillberg[6], G. Ginther[50,71], B. Gómez[8], A. Goussiou[82], P.D. Grannis[72], S. Greder[19], H. Greenlee[50], Z.D. Greenwood[60], E.M. Gregores[4], G. Grenier[20], Ph. Gris[13], J.-F. Grivaz[16], A. Grohsjean[26], S. Grünendahl[50], M.W. Grünewald[31], F. Guo[72], J. Guo[72], G. Gutierrez[50], P. Gutierrez[75], A. Haas[70], N.J. Hadley[61], P. Haefner[26], S. Hagopian[49], J. Haley[68], I. Hall[65], R.E. Hall[47], L. Han[7], K. Harder[45], A. Harel[71], J.M. Hauptman[57], J. Hays[44], T. Hebbeker[21], D. Hedin[52], J.G. Hegeman[35], A.P. Heinson[48], U. Heintz[62], C. Hensel[24], I. Heredia-De La Cruz[34], K. Herner[64], G. Hesketh[63], M.D. Hildreth[55], R. Hirosky[81], T. Hoang[49], J.D. Hobbs[72], B. Hoeneisen[12], M. Hohlfeld[22], S. Hossain[75], P. Houben[35], Y. Hu[72], Z. Hubacek[10], N. Huske[17], V. Hynek[10], I. Iashvili[69], R. Illingworth[50], A.S. Ito[50], S. Jabeen[62], M. Jaffré[16], S. Jain[75], K. Jakobs[23], D. Jamin[15], C. Jarvis[61], R. Jesik[44], K. Johns[46], C. Johnson[70], M. Johnson[50], D. Johnston[67], A. Jonckheere[50], P. Jonsson[44], A. Juste[50], E. Kajfasz[15], D. Karmanov[39], P.A. Kasper[50], I. Katsanos[67], V. Kaushik[78], R. Kehoe[79], S. Kermiche[15], N. Khalatyan[50], A. Khanov[76], A. Kharchilava[69], Y.N. Kharzheev[37], D. Khatidze[70], T.J. Kim[32], M.H. Kirby[53], M. Kirsch[21], B. Klima[50], J.M. Kohli[28], J.-P. Konrath[23], A.V. Kozelov[40], J. Kraus[65], T. Kuhl[25], A. Kumar[69], A. Kupco[11], T. Kurča[20], V.A. Kuzmin[39], J. Kvita[9], F. Lacroix[13], D. Lam[55], S. Lammers[54], G. Landsberg[77], P. Lebrun[20], W.M. Lee[50], A. Leflat[39], J. Lellouch[17], J. Li[78,‡], L. Li[48], Q.Z. Li[50], S.M. Lietti[5], J.K. Lim[32], D. Lincoln[50], J. Linnemann[65], V.V. Lipaev[40], R. Lipton[50], Y. Liu[7], Z. Liu[6], A. Lobodenko[41], M. Lokajicek[11], P. Love[43], H.J. Lubatti[82], R. Luna-Garcia[34,d], A.L. Lyon[50], A.K.A. Maciel[2], D. Mackin[80], P. Mättig[27], A. Magerkurth[64], P.K. Mal[82], H.B. Malbouisson[3], S. Malik[67], V.L. Malyshev[37], Y. Maravin[59], B. Martin[14], R. McCarthy[72], C.L. McGivern[58], M.M. Meijer[36], A. Melnitchouk[66], L. Mendoza[8], D. Menezes[52], P.G. Mercadante[5], M. Merkin[39], K.W. Merritt[50], A. Meyer[21], J. Meyer[24], J. Mitrevski[70], R.K. Mommsen[45], N.K. Mondal[30], R.W. Moore[6], T. Moulik[58], G.S. Muanza[15], M. Mulhearn[70], O. Mundal[22], L. Mundim[3], E. Nagy[15], M. Naimuddin[50], M. Narain[77], H.A. Neal[64], J.P. Negret[8], P. Neustroev[41], H. Nilsen[23], H. Nogima[3], S.F. Novaes[5], T. Nunnemann[26], G. Obrant[41], C. Ochando[16], D. Onoprienko[59], J. Orduna[34], N. Oshima[50], N. Osman[44], J. Osta[55], R. Otec[10], G.J. Otero y Garzón[1], M. Owen[45], M. Padilla[48], P. Padley[80], M. Pangilinan[77], N. Parashar[56], S.-J. Park[24], S.K. Park[32], J. Parsons[70], R. Partridge[77], N. Parua[54], A. Patwa[73], G. Pawloski[80], B. Penning[23], M. Perfilov[39], K. Peters[45], Y. Peters[45], P. Pétroff[16], R. Piegaia[1], J. Piper[65], M.-A. Pleier[22], P.L.M. Podesta-Lerma[34,e], V.M. Podstavkov[50], Y. Pogorelov[55], M.-E. Pol[2], P. Polozov[38], A.V. Popov[40], C. Potter[6], W.L. Prado da Silva[3], S. Protopopescu[73], J. Qian[64], A. Quadt[24], B. Quinn[66], A. Rakitine[43], M.S. Rangel[16], K. Ranjan[29], P.N. Ratoff[43], P. Renkel[79], P. Rich[45], M. Rijssenbeek[72], I. Ripp-Baudot[19],

F. Rizatdinova[76], S. Robinson[44], R.F. Rodrigues[3], M. Rominsky[75], C. Royon[18], P. Rubinov[50], R. Ruchti[55], G. Safronov[38], G. Sajot[14], A. Sánchez-Hernández[34], M.P. Sanders[17], B. Sanghi[50], G. Savage[50], L. Sawyer[60], T. Scanlon[44], D. Schaile[26], R.D. Schamberger[72], Y. Scheglov[41], H. Schellman[53], T. Schliephake[27], S. Schlobohm[82], C. Schwanenberger[45], R. Schwienhorst[65], J. Sekaric[49], H. Severini[75], E. Shabalina[24], M. Shamim[59], V. Shary[18], A.A. Shchukin[40], R.K. Shivpuri[29], V. Siccardi[19], V. Simak[10], V. Sirotenko[50], P. Skubic[75], P. Slattery[71], D. Smirnov[55], G.R. Snow[67], J. Snow[74], S. Snyder[73], S. Söldner-Rembold[45], L. Sonnenschein[21], A. Sopczak[43], M. Sosebee[78], K. Soustruznik[9], B. Spurlock[78], J. Stark[14], V. Stolin[38], D.A. Stoyanova[40], J. Strandberg[64], S. Strandberg[42], M.A. Strang[69], E. Strauss[72], M. Strauss[75], R. Ströhmer[26], D. Strom[53], L. Stutte[50], S. Sumowidagdo[49], P. Svoisky[36], M. Takahashi[45], A. Tanasijczuk[1], W. Taylor[6], B. Tiller[26], F. Tissandier[13], M. Titov[18], V.V. Tokmenin[37], I. Torchiani[23], D. Tsybychev[72], B. Tuchming[18], C. Tully[68], P.M. Tuts[70], R. Unalan[65], L. Uvarov[41], S. Uvarov[41], S. Uzunyan[52], B. Vachon[6], P.J. van den Berg[35], R. Van Kooten[54], W.M. van Leeuwen[35], N. Varelas[51], E.W. Varnes[46], I.A. Vasilyev[40], P. Verdier[20], L.S. Vertogradov[37], M. Verzocchi[50], D. Vilanova[18], P. Vint[44], P. Vokac[10], M. Voutilainen[67,f], R. Wagner[68], H.D. Wahl[49], M.H.L.S. Wang[71], J. Warchol[55], G. Watts[82], M. Wayne[55], G. Weber[25], M. Weber[50,g], L. Welty-Rieger[54], A. Wenger[23,h], M. Wetstein[61], A. White[78], D. Wicke[25], M.R.J. Williams[43], G.W. Wilson[58], S.J. Wimpenny[48], M. Wobisch[60], D.R. Wood[63], T.R. Wyatt[45], Y. Xie[77], C. Xu[64], S. Yacoob[53], R. Yamada[50], W.-C. Yang[45], T. Yasuda[50], Y.A. Yatsunenko[37], Z. Ye[50], H. Yin[7], K. Yip[73], H.D. Yoo[77], S.W. Youn[53], J. Yu[78], C. Zeitnitz[27], S. Zelitch[81], T. Zhao[82], B. Zhou[64], J. Zhu[72], M. Zielinski[71], D. Zieminska[54], L. Zivkovic[70], V. Zutshi[52], and E.G. Zverev[39]

(The DØ Collaboration)

[1] *Universidad de Buenos Aires, Buenos Aires, Argentina*
[2] *LAFEX, Centro Brasileiro de Pesquisas Físicas, Rio de Janeiro, Brazil*
[3] *Universidade do Estado do Rio de Janeiro, Rio de Janeiro, Brazil*
[4] *Universidade Federal do ABC, Santo André, Brazil*
[5] *Instituto de Física Teórica, Universidade Estadual Paulista, São Paulo, Brazil*
[6] *University of Alberta, Edmonton, Alberta, Canada; Simon Fraser University, Burnaby, British Columbia, Canada; York University, Toronto, Ontario, Canada and McGill University, Montreal, Quebec, Canada*
[7] *University of Science and Technology of China, Hefei, People's Republic of China*
[8] *Universidad de los Andes, Bogotá, Colombia*
[9] *Center for Particle Physics, Charles University, Faculty of Mathematics and Physics, Prague, Czech Republic*
[10] *Czech Technical University in Prague, Prague, Czech Republic*
[11] *Center for Particle Physics, Institute of Physics, Academy of Sciences of the Czech Republic, Prague, Czech Republic*
[12] *Universidad San Francisco de Quito, Quito, Ecuador*
[13] *LPC, Université Blaise Pascal, CNRS/IN2P3, Clermont, France*
[14] *LPSC, Université Joseph Fourier Grenoble 1, CNRS/IN2P3, Institut National Polytechnique de Grenoble, Grenoble, France*
[15] *CPPM, Aix-Marseille Université, CNRS/IN2P3, Marseille, France*
[16] *LAL, Université Paris-Sud, IN2P3/CNRS, Orsay, France*
[17] *LPNHE, IN2P3/CNRS, Universités Paris VI and VII, Paris, France*
[18] *CEA, Irfu, SPP, Saclay, France*
[19] *IPHC, Université de Strasbourg, CNRS/IN2P3, Strasbourg, France*
[20] *IPNL, Université Lyon 1, CNRS/IN2P3, Villeurbanne, France and Université de Lyon, Lyon, France*
[21] *III. Physikalisches Institut A, RWTH Aachen University, Aachen, Germany*
[22] *Physikalisches Institut, Universität Bonn, Bonn, Germany*
[23] *Physikalisches Institut, Universität Freiburg, Freiburg, Germany*
[24] *II. Physikalisches Institut, Georg-August-Universität G Göttingen, Germany*
[25] *Institut für Physik, Universität Mainz, Mainz, Germany*
[26] *Ludwig-Maximilians-Universität München, München, Germany*
[27] *Fachbereich Physik, University of Wuppertal, Wuppertal, Germany*
[28] *Panjab University, Chandigarh, India*
[29] *Delhi University, Delhi, India*
[30] *Tata Institute of Fundamental Research, Mumbai, India*
[31] *University College Dublin, Dublin, Ireland*
[32] *Korea Detector Laboratory, Korea University, Seoul, Korea*
[33] *SungKyunKwan University, Suwon, Korea*
[34] *CINVESTAV, Mexico City, Mexico*
[35] *FOM-Institute NIKHEF and University of Amsterdam/NIKHEF, Amsterdam, The Netherlands*

[36] Radboud University Nijmegen/NIKHEF, Nijmegen, The Netherlands
[37] Joint Institute for Nuclear Research, Dubna, Russia
[38] Institute for Theoretical and Experimental Physics, Moscow, Russia
[39] Moscow State University, Moscow, Russia
[40] Institute for High Energy Physics, Protvino, Russia
[41] Petersburg Nuclear Physics Institute, St. Petersburg, Russia
[42] Stockholm University, Stockholm, Sweden, and Uppsala University, Uppsala, Sweden
[43] Lancaster University, Lancaster, United Kingdom
[44] Imperial College, London, United Kingdom
[45] University of Manchester, Manchester, United Kingdom
[46] University of Arizona, Tucson, Arizona 85721, USA
[47] California State University, Fresno, California 93740, USA
[48] University of California, Riverside, California 92521, USA
[49] Florida State University, Tallahassee, Florida 32306, USA
[50] Fermi National Accelerator Laboratory, Batavia, Illinois 60510, USA
[51] University of Illinois at Chicago, Chicago, Illinois 60607, USA
[52] Northern Illinois University, DeKalb, Illinois 60115, USA
[53] Northwestern University, Evanston, Illinois 60208, USA
[54] Indiana University, Bloomington, Indiana 47405, USA
[55] University of Notre Dame, Notre Dame, Indiana 46556, USA
[56] Purdue University Calumet, Hammond, Indiana 46323, USA
[57] Iowa State University, Ames, Iowa 50011, USA
[58] University of Kansas, Lawrence, Kansas 66045, USA
[59] Kansas State University, Manhattan, Kansas 66506, USA
[60] Louisiana Tech University, Ruston, Louisiana 71272, USA
[61] University of Maryland, College Park, Maryland 20742, USA
[62] Boston University, Boston, Massachusetts 02215, USA
[63] Northeastern University, Boston, Massachusetts 02115, USA
[64] University of Michigan, Ann Arbor, Michigan 48109, USA
[65] Michigan State University, East Lansing, Michigan 48824, USA
[66] University of Mississippi, University, Mississippi 38677, USA
[67] University of Nebraska, Lincoln, Nebraska 68588, USA
[68] Princeton University, Princeton, New Jersey 08544, USA
[69] State University of New York, Buffalo, New York 14260, USA
[70] Columbia University, New York, New York 10027, USA
[71] University of Rochester, Rochester, New York 14627, USA
[72] State University of New York, Stony Brook, New York 11794, USA
[73] Brookhaven National Laboratory, Upton, New York 11973, USA
[74] Langston University, Langston, Oklahoma 73050, USA
[75] University of Oklahoma, Norman, Oklahoma 73019, USA
[76] Oklahoma State University, Stillwater, Oklahoma 74078, USA
[77] Brown University, Providence, Rhode Island 02912, USA
[78] University of Texas, Arlington, Texas 76019, USA
[79] Southern Methodist University, Dallas, Texas 75275, USA
[80] Rice University, Houston, Texas 77005, USA
[81] University of Virginia, Charlottesville, Virginia 22901, USA and
[82] University of Washington, Seattle, Washington 98195, USA

(Dated: March 31, 2009)

We combine measurements of the top quark pair production cross section in $p\bar{p}$ collisions in the ℓ+jets, $\ell\ell$ and $\tau\ell$ final states (where ℓ is an electron or muon) at a center of mass energy of $\sqrt{s} = 1.96$ TeV in 1 fb^{-1} of data collected with the D0 detector. For a top quark mass of 170 GeV, we obtain $\sigma_{t\bar{t}} = 8.18^{+0.98}_{-0.87}$ pb. In addition, the ratios of $t\bar{t}$ cross sections in different final states are used to set upper limits on the branching fractions $B(t \to H^+b \to \tau^+\nu b)$ and $B(t \to H^+b \to c\bar{s}b)$ as a function of charged Higgs boson mass. Based on predictions from higher order quantum chromodynamics, we extract a mass for the top quark from the combined $t\bar{t}$ cross section.

PACS numbers: 12.15.Ff, 13.85.Lg, 13.85.Qk, 13.85.Rm, 14.65.Ha, 14.80.Cp

Precise measurements of the production and decay properties of the heaviest known fermion, the top quark, provide important tests of the standard model (SM) and offer a window for searches for new physics. The inclusive top-antitop quark pair ($t\bar{t}$) production cross section ($\sigma_{t\bar{t}}$) is measured in different $t\bar{t}$ decay channels assuming SM branching fractions. The results are compared to predictions in next-to-leading order perturbative quan-

tum chromodynamics (QCD), including higher order soft gluon resummations [1–4]. Ratios of $\sigma_{t\bar{t}}$ measured in different final states are particularly sensitive to non-SM particles that may appear in top quark decays, especially if the boson in the decay is not a SM W boson. An example is the decay into a charged Higgs boson ($t \to H^+ b$), which, as predicted in some models [5], can compete with the SM decay $t \to W^+ b$. Additionally, many experimental uncertainties cancel in the ratios. Furthermore, since $\sigma_{t\bar{t}}$ depends on the mass of the top quark (m_t), it can be used to extract m_t. Such measurement is less accurate than direct mass measurements, but provides complementary information.

Within the SM, each quark of the $t\bar{t}$ pair is expected to decay nearly 100% of the times into a W boson and a b quark [6]. W bosons can decay hadronically into $q\bar{q}'$ pairs or leptonically into $e\nu_e$, $\mu\nu_\mu$ and $\tau\nu_{tau}$ with the τ in turn decaying onto an electron, a muon or hadrons, and associated neutrinos. If one of the W bosons decays hadronically while the other one produces a direct electron or muon or a secondary electron or muon from τ decay, the final state is referred to as the ℓ+jets channel. The leptonic decay of both W bosons leads to either a dilepton final state containing a pair of electrons, a pair of muons, or an electron and a muon (the $\ell\ell$ channel), or a hadronically decaying tau accompanied either by an electron or a muon (the $\tau\ell$ channel).

Measurements of the individual $t\bar{t}$ cross sections in $\ell\ell$ and $\tau\ell$ channels using about 1 fb^{-1} of $p\bar{p}$ data from the D0 detector at the Fermilab Tevatron collider at $\sqrt{s} =$ 1.96 TeV are available in Ref. [7]. In the ℓ+jets channel, we use the same selection and background estimation as in Ref. [8], but a slightly larger dataset and a unified treatment of systematic uncertainties with the $\ell\ell$ and $\tau\ell$ channels. We provide a brief summary of the event selection and analysis procedures below.

In each final state we select data samples enriched in $t\bar{t}$ events by requiring one (two) isolated high transverse momentum (p_T) lepton for the ℓ+jets ($\ell\ell$) channel. At least two (three) high p_T jets are required for $\ell\ell$ and $\tau\ell$ (ℓ+jets) events. Further, in all but the $e\mu$ channel, large transverse missing energy ($\not\!\!E_T$) is required to account for the large transverse momenta of neutrinos from W boson or τ lepton decays. In the $e\mu$ final state, a requirement on the sum of p_T of the highest p_T (leading) lepton and the two leading jets is imposed instead. In the $\mu\mu$ channel, the $\not\!\!E_T$ requirement is supplemented with a requirement on the significance of the $\not\!\!E_T$ measurement, estimated from the p_T of muons and jets, and their expected resolutions. Additional criteria are applied on the invariant mass of the two opposite charge leptons of the same flavor in the ee and $\mu\mu$ channels to reduce the dominant background from $Z/\gamma^* \to \ell^+\ell^-$ events. In the ℓ+jets and $\tau\ell$ channels we require a minimum azimuthal angle separation between the $\not\!\!E_T$ vector and the lepton p_T, $\Delta\phi(\ell, \not\!\!E_T)$, to reduce background from multijet events, where jets are misidentified as electron, muon or τ. Details of lepton, jet and $\not\!\!E_T$ identification are provided in Refs. [9, 10]. The final selection in these channels demands at least one identified b jet via a neural-network based algorithm [11]. In the ℓ+jets channel we separate events with one or ≥ 2 b-tagged jets due to their different signal over background ratio and systematic uncertainties.

To simplify the combination and extraction of cross section ratios, all channels are constructed to be exclusive. If a reconstructed event can enter two selected samples, we keep it in the sample having less expected events. This is achieved by excluding events containing any isolated electrons in the $\mu\mu$ channel, a second electron in the $e\mu$ channel, or a muon or a second electron in the e+jets channel. Because of different muon identification criteria applied in the different channels, we reject those events from the μ+jets channel that pass the $\mu\mu$ selection or contain an electron. In the $\tau\ell$ channel we allow the signal to contain events from the ℓ+jets final state, and reject these events in the ℓ+jets channel. Finally, the τe channel and the $\ell\ell$ channels are kept statistically independent by rejecting events with a muon or a second electron in the τe selection. For the $\tau\mu$ channel, as in μ+jets, we reject events that pass the $\mu\mu$ selection or contain an electron.

The compositions of the samples in the ℓ+jets, $\ell\ell$ and $\tau\ell$ channels are shown in Table I. W+jets production dominates the background for the ℓ+jets events, while multijet production is the most important background in the $\tau\ell$ channel. Background in the $\ell\ell$ channels comes mainly from Z+jets production. The smaller contribution from diboson production is included in the category labeled "other background". This category also includes the contribution from single top quark production in the ℓ+jets and $\tau\ell$ channels.

To calculate the combined cross section, we define a joint likelihood function as the product of Poisson probabilities for the 14 disjoint subsamples, as listed in Table I. Fourteen additional Poisson terms constrain the multijet background in the ℓ+jets and $\tau\ell$ channels. In particular, for the τe and $\tau\mu$ channels, the multijet background is determined by counting events with an electron or muon and associated τ of the same electric charge, introducing a corresponding Poisson term per channel. In the ℓ+jets channel, we estimate the multijet background separately for each of the eight subchannels by using corresponding control data samples [12]. Four additional terms arise from applying this same method in evaluating the multijet background before b tagging.

Systematic uncertainties are included in the likelihood function through "nuisance" parameters [12], in which each independent source of systematic uncertainty is modeled by one free parameter. Each of these parameters is represented by a Gaussian probability density function with zero mean and width corresponding to one standard deviation (sd) of the parameter uncertainty; all are allowed to float in the maximization of the likelihood function, thereby changing the central value of the measured $\sigma_{t\bar{t}}$. Thus, the likelihood function to be maximized

TABLE I: Expected numbers of background and signal events for $\sigma_{t\bar{t}} = 8.18$ pb, observed numbers of data events and measured $\sigma_{t\bar{t}}$ at top mass of 170 GeV. Quoted uncertainties include both statistical and systematic uncertainties, added in quadrature.

Channel	Luminosity(pb^{-1})	W+jets	Z+jets	Multijet	Other bkg	$t\bar{t}$	Total	Observed	$\sigma_{t\bar{t}}$ (pb)
e+jets (3 jets, 1 b tag)	1038	$53.4^{+6.0}_{-6.0}$	$6.0^{+1.2}_{-1.2}$	$31.5^{+3.5}_{-3.5}$	$11.4^{+1.5}_{-1.4}$	$81.7^{+6.4}_{-6.7}$	$184.0^{+9.0}_{-9.2}$	183	$8.06^{+1.89}_{-1.71}$
μ+jets (3 jets, 1 b tag)	996	$59.2^{+5.5}_{-5.6}$	$6.5^{+1.3}_{-1.3}$	$9.7^{+2.8}_{-2.8}$	$9.5^{+1.2}_{-1.2}$	$59.0^{+5.7}_{-5.6}$	$143.9^{+8.1}_{-8.1}$	133	$6.43^{+2.22}_{-2.01}$
e+jets (3 jets, ≥ 2 b tags)	1038	$5.0^{+0.8}_{-0.8}$	$0.6^{+0.2}_{-0.2}$	$2.7^{+0.3}_{-0.3}$	$2.4^{+0.4}_{-0.4}$	$30.7^{+3.9}_{-3.9}$	$41.5^{+4.7}_{-4.6}$	40	$7.78^{+2.41}_{-2.01}$
μ+jets (3 jets, ≥ 2 b tags)	996	$5.8^{+0.9}_{-0.9}$	$0.7^{+0.2}_{-0.2}$	$1.0^{+0.3}_{-0.3}$	$2.1^{+0.3}_{-0.3}$	$23.8^{+3.4}_{-3.2}$	$33.5^{+4.1}_{-3.9}$	31	$7.29^{+2.73}_{-2.25}$
e+jets (≥ 4 jets, 1 b tag)	1038	$8.5^{+2.7}_{-2.7}$	$2.2^{+0.5}_{-0.5}$	$7.9^{+1.0}_{-1.0}$	$3.0^{+0.5}_{-0.5}$	$81.6^{+8.7}_{-9.1}$	$103.3^{+7.3}_{-7.6}$	113	$9.38^{+1.82}_{-1.52}$
μ+jets (≥ 4 jets, 1 b tag)	996	$13.6^{+2.6}_{-2.7}$	$2.5^{+0.7}_{-0.6}$	$0.0^{+0.0}_{-0.0}$	$2.4^{+0.4}_{-0.4}$	$65.9^{+6.9}_{-7.2}$	$84.3^{+5.9}_{-6.3}$	99	$10.44^{+2.11}_{-1.76}$
e+jets (≥ 4 jets, ≥ 2 b tags)	1038	$1.0^{+0.3}_{-0.3}$	$0.2^{+0.1}_{-0.1}$	$1.1^{+0.1}_{-0.1}$	$0.9^{+0.2}_{-0.2}$	$41.7^{+6.0}_{-6.0}$	$44.9^{+6.0}_{-6.0}$	30	$5.12^{+1.59}_{-1.28}$
μ+jets (≥ 4 jets, ≥ 2 b tags)	996	$1.5^{+0.4}_{-0.4}$	$0.3^{+0.1}_{-0.1}$	$0.0^{+0.0}_{-0.0}$	$0.7^{+0.1}_{-0.1}$	$35.6^{+5.0}_{-5.1}$	$38.2^{+5.1}_{-5.2}$	34	$7.60^{+2.11}_{-1.70}$
ee	1074		$2.3^{+0.5}_{-0.5}$	$0.6^{+0.4}_{-0.4}$	$0.5^{+0.1}_{-0.1}$	$11.6^{+1.2}_{-1.2}$	$15.0^{+1.5}_{-1.5}$	17	$9.61^{+3.47}_{-2.84}$
$e\mu$ (1 jet)	1070		$5.5^{+0.7}_{-0.8}$	$0.9^{+0.3}_{-0.2}$	$3.1^{+0.7}_{-0.7}$	$8.9^{+1.4}_{-1.4}$	$18.4^{+1.9}_{-1.9}$	21	$10.61^{+5.33}_{-4.23}$
$e\mu$ (≥ 2 jets)	1070		$5.4^{+0.9}_{-1.0}$	$2.6^{+0.6}_{-0.5}$	$1.4^{+0.4}_{-0.4}$	$36.4^{+3.6}_{-3.6}$	$45.8^{+4.5}_{-4.5}$	39	$6.66^{+1.81}_{-1.52}$
$\mu\mu$	1009		$5.6^{+1.1}_{-1.2}$	$0.2^{+0.2}_{-0.2}$	$0.6^{+0.1}_{-0.1}$	$9.1^{+1.0}_{-1.0}$	$15.4^{+1.8}_{-1.9}$	12	$5.08^{+3.82}_{-3.06}$
τe	1038	$0.6^{+0.0}_{-0.1}$	$0.6^{+0.1}_{-0.1}$	$3.0^{+1.7}_{-1.7}$	$0.2^{+0.1}_{-0.1}$	$10.7^{+1.3}_{-1.3}$	$15.0^{+2.2}_{-2.2}$	16	$8.94^{+4.03}_{-3.32}$
$\tau\mu$	996	$0.8^{+0.1}_{-0.2}$	$1.2^{+0.3}_{-0.3}$	$8.0^{+2.8}_{-2.8}$	$0.2^{+0.0}_{-0.0}$	$12.6^{+1.4}_{-1.4}$	$22.7^{+3.2}_{-3.2}$	20	$6.40^{+3.88}_{-3.43}$

can be represented by the product

$$\mathcal{L} = \prod_{i=1}^{14} \mathcal{P}(n_i, m_i) \times \prod_{j=1}^{14} \mathcal{P}(n_j, m_j) \times \prod_{k=1}^{K} \mathcal{G}(\nu_k; 0, \mathrm{sd}) \,, \quad (1)$$

where $\mathcal{P}(n, m)$ is the Poisson probability to observe n events given the expectation of m events. The predicted number of events in each channel is the sum of the predicted background and expected $t\bar{t}$ events, which depends on $\sigma_{t\bar{t}}$. In the product, i runs over the subsamples, and j runs over the multijet background subsamples. The Gaussian distributions $\mathcal{G}(\nu_k; 0, \mathrm{sd})$ describe the systematic uncertainties, where K is the total number of independent sources of systematic uncertainty, and ν_k are the individual nuisance parameters. Correlations are taken into account, by using the same nuisance parameter for the same source of systematic uncertainty in different channels.

Systematic uncertainties on the measured $\sigma_{t\bar{t}}$ are evaluated from sources that include electron and muon identification; τ and jet identification and energy calibration; b-jet identification; modeling of triggers, signal and background; and integrated luminosity. All these uncertainties are treated as fully correlated among channels and between signal and background. Systematic uncertainties arising from limited statistics of data or Monte Carlo samples used in estimating signal or backgrounds are considered to be uncorrelated. A detailed discussion on systematic uncertainties can be found in Refs. [7, 8]. Table II shows a breakdown of uncertainties on the combined cross section. We evaluate the effect from each source by setting all uncertainties to zero except the one in question and redoing the likelihood maximization with respect to only the corresponding nuisance parameter. Since the method allows each uncertainty to change the central value, the total uncertainty on $\sigma_{t\bar{t}}$ differs slightly from the quadratic sum of the statistical and individual systematic uncertainties. The total systematic uncertainty on $\sigma_{t\bar{t}}$ exceeds the statistical contribution. The luminosity uncertainty of 6.1% which enters into the estimation of the majority of the backgrounds and the luminosity measurement of the selected samples is the dominant source of systematic uncertainty.

Table III summarizes the individual $\sigma_{t\bar{t}}$ measurements for the individual channels, as well as some of their combinations. Within uncertainties, all measurements are consistent with each other. The combined cross section for ℓ+jets, $\ell\ell$ and $\tau\ell$ final states for a top quark mass of 170 GeV is evaluated to be

$$\sigma_{t\bar{t}} = 8.18^{+0.98}_{-0.87} \text{ pb} \,, \quad (2)$$

in agreement with theoretical predictions [1–4]. The observed number of events in the different channels is compared to the sum of the background and combined $t\bar{t}$ signal in Fig. 1(a).

We compute ratios R_σ of measured cross sections, $R_\sigma^{\ell\ell/\ell j} = \sigma_{t\bar{t}}^{\ell\ell}/\sigma_{t\bar{t}}^{\ell+\mathrm{jets}}$ and $R_\sigma^{\tau\ell/\ell\ell\text{-}\ell j} = \sigma_{t\bar{t}}^{\tau_\ell}/\sigma_{t\bar{t}}^{\ell+\mathrm{jets}\&\ell\ell}$, by generating pseudo-datasets in the numerator and denominator. $\sigma_{t\bar{t}}^{\mathrm{channel}}$ represent the measured cross sections in the corresponding channel. The pseudo-datasets are created by varying the number of signal and background events around the expected number according to Poisson probabilities. All independent sources of systematic uncertainties are varied within a Gaussian distribution. Although the individual channels considered are exclusive, each channel can receive signal contributions from different $t\bar{t}$ decay modes. We take into account the contribution of signal from dilepton into the ℓ+jets final

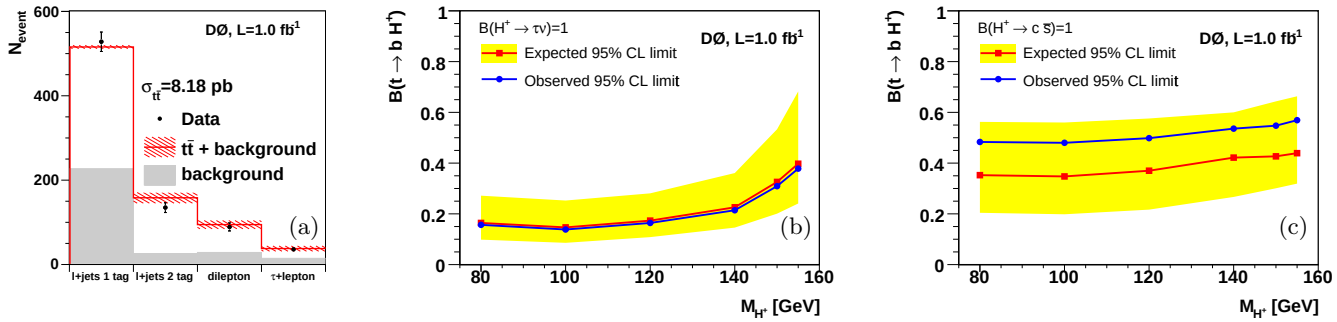

FIG. 1: (a) Expected and observed numbers of events versus channel, used in measuring the combined $\sigma_{t\bar{t}}$. The dashed band around the prediction indicates the total uncertainty. Upper limits on $B(t \to H^+b)$ for (b) tauonic and (c) leptophobic H^+ decays. The yellow band shows the ± 1 sd band around the expected limit.

TABLE II: Summary of uncertainties on the combined $\sigma_{t\bar{t}}$.

Source	$\Delta\sigma_{t\bar{t}}$ (pb)
Statistical	$+0.47\ -0.46$
Lepton identification	$+0.15\ -0.14$
Tau identification	$+0.02\ -0.02$
Jet identification	$+0.11\ -0.11$
Jet energy scale	$+0.19\ -0.16$
Tau energy scale	$+0.02\ -0.02$
Trigger modeling	$+0.11\ -0.07$
b jet identification	$+0.34\ -0.32$
Signal modeling	$+0.17\ -0.15$
Background estimation	$+0.14\ -0.14$
Multijet background	$+0.12\ -0.12$
Luminosity	$+0.56\ -0.48$
Other	$+0.15\ -0.14$
Total systematic uncertainty	$+0.78\ -0.69$

TABLE III: Summary of measured $\sigma_{t\bar{t}}$ in different channels for $m_t = 170$ GeV.

Channel	$\sigma_{t\bar{t}}$ (pb)
ℓ+jets	$8.46^{+1.09}_{-0.97}$
$\ell\ell$ [7]	$7.46^{+1.60}_{-1.37}$
ℓ+jets and $\ell\ell$	$8.18^{+0.99}_{-0.87}$
$\tau\ell$ [7]	$7.77^{+2.90}_{-2.47}$
ℓ+jets, $\ell\ell$ and $\tau\ell$	$8.18^{+0.98}_{-0.87}$

state as well as the dilepton and ℓ+jets into the $\tau\ell$ channel by using the corresponding observed individual cross sections in generating the pseudo-datasets. For each pseudo-dataset, we perform the maximization of Eq. 1 separately in the numerator and denominator, and divide the results. The central value is obtained from the mode of the distribution of R_σ, and the uncertainties are derived from the interval containing 68% of the pseudo-experiments. From these pseudo-experiments we obtain $R_\sigma^{\ell\ell/\ell j} = 0.86^{+0.19}_{-0.17}$ and $R_\sigma^{\tau\ell/\ell\ell\text{-}\ell j} = 0.97^{+0.32}_{-0.29}$, which is consistent with the SM expectation of $R_\sigma = 1$.

We use these ratios to extract upper limits on the branching ratio $B := B(t \to H^+b)$. In particular, a charged Higgs boson decaying into a tau and a neutrino ($B(H^+ \to \tau\nu) = 1$) results in more events in the $\tau\ell$ channel, while fewer events appear in the $\ell\ell$ and ℓ+jets final states compared to the SM prediction. In case of the leptophobic ($B(H^+ \to c\bar{s}) = 1$) model, the number of dilepton events decreases faster than the number of ℓ+jets events for increasing $B(t \to H^+b)$. We therefore use $R_\sigma^{\ell\ell/\ell j}$ to set limits on the leptophobic model, while $R_\sigma^{\tau\ell/\ell\ell\text{-}\ell j}$ is explored to search for decays in which the charged Higgs bosons are assumed to decay exclusively to taus.

To extract the limits, we generate pseudo-datasets assuming different branching fractions $B(t \to H^+b)$. The signal for a charged Higgs boson is simulated using the PYTHIA Monte Carlo event generator [13], and includes decays of $t\bar{t} \to W^+bH^-\bar{b}$ (and its charge conjugate) and $t\bar{t} \to H^+bH^-\bar{b}$. For a given branching fraction B, we calculate the expected number of $t\bar{t}$ events per final state,

$$N_{t\bar{t}} = [(1-B)^2 \cdot \epsilon_{t\bar{t}\to W^+bW^-\bar{b}} + 2B(1-B) \cdot \epsilon_{t\bar{t}\to W^+bH^-\bar{b}} + B^2 \cdot \epsilon_{t\bar{t}\to H^+bH^-\bar{b}}]\sigma_{t\bar{t}}L\,, \quad (3)$$

with ϵ are the selection efficiencies for the different decays and L is the integrated luminosity. We add $N_{t\bar{t}}$ to the expected background and treat the sum as a new number of expected events in each channel. We then perform the likelihood maximization to extract $\sigma_{t\bar{t}}$ from these pseudo-data as if they contained only SM $t\bar{t}$ production. This provides different distributions for the ratios of cross sections for each generated B, which are compared to the observed ratio. We set limits on B by using the frequentist approach of Feldman and Cousins [14].

From $R_\sigma^{\tau\ell/\ell\ell\text{-}\ell j}$ we extract B in the tauonic model, and we use $R_\sigma^{\ell\ell/\ell j}$ to get B for the leptophobic charged Higgs boson decays. The observed and expected (i.e., for $R_\sigma = 1$) limits for the tauonic and the leptophobic charged Higgs boson models are shown in Figs. 1b and 1c, respectively. In the tauonic model the upper limits on B range from 15% to 40% for charged Higgs boson masses between 80 GeV and 155 GeV, for a leptophobic charged

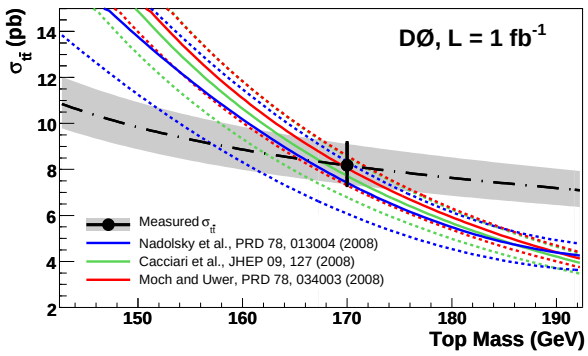

FIG. 2: Experimental and theoretical [1–3] $\sigma_{t\bar{t}}$ as function of m_t. The point shows the measured combined $\sigma_{t\bar{t}}$, the black dashed line the fit with Eq. 4 and the gray band the corresponding total experimental uncertainty.

Higgs boson the limit is smaller than 57% for the same range of charged Higgs boson masses.

The interpretation of the direct measurement of the top quark mass [6], has become a subject of intense discussion in terms of its renormalization scheme [15]. The extraction of this parameter from the measured cross section provides complementary information, with different sensitivity to theoretical and experimental uncertainties, relative to direct methods that rely on kinematic details of the reconstruction of the top quarks. Using simulated samples of $t\bar{t}$ events generated at different values of the top quark mass, taking into account the mass dependence of the selection efficiencies, we fit the combined $\sigma_{t\bar{t}}$ as a function of m_t:

$$\sigma_{t\bar{t}}(m_t) = \frac{1}{m_t^4}[a+b(m_t-m_0)+c(m_t-m_0)^2+d(m_t-m_0)^3] \quad (4)$$

where $\sigma_{t\bar{t}}$ and m_t are in pb and GeV, respectively, and $m_0 = 170$ GeV [16].

We compare this parameterization to a prediction in pure next-to-leading-order (NLO) QCD [1], to a calculation including NLO QCD and all higher-order soft-gluon resummations in next-to-leading logarithms (NLL) [2], to an approximation to the next-to-next-to-leading-order (NNLO) QCD cross section that includes all next-to-next-to-leading logarithms (NNLL) relevant in NNLO QCD [3], and to a calculation that employs full kinematics in the double differential cross section beyond NLL using the soft anomalous dimension matrix to calculate the soft-gluon contributions at NNLO [4]. Figure 2 shows the experimental and the theoretical [1–3] $t\bar{t}$ cross sections as a function of the top quark mass.

Following the method of Refs. [7, 8], we extract the most probable top quark mass values and the 68% CL band. Since the theoretical predictions are performed in the pole mass scheme, this defines the extracted parameter here. The results are given in Table IV. All values are in good agreement with the current world average of 171.2 ± 2.1 GeV [6].

TABLE IV: Top quark mass with 68% CL region for different theoretical predictions of $\sigma_{t\bar{t}}$. Combined experimental and theoretical uncertainties are shown.

Theoretical prediction	m_t (GeV)
NLO [1]	$165.5^{+6.1}_{-5.9}$
NLO+NLL [2]	$167.5^{+5.8}_{-5.6}$
approximate NNLO [3]	$169.1^{+5.9}_{-5.2}$
approximate NNLO [4]	$168.2^{+5.9}_{-5.4}$

In summary, we have combined the $t\bar{t}$ cross section measurements in ℓ+jets, $\ell\ell$ and $\tau\ell$ channels to measure $\sigma_{t\bar{t}} = 8.18^{+0.98}_{-0.87}$ pb for a top quark mass of 170 GeV. We have also calculated ratios of cross sections and interpreted them in terms of limits on non-standard model top quark decays into a charged Higgs boson. All results are in good agreement with the SM expectations. Finally, using different theoretical predictions given in the pole mass scheme, we have extracted the top quark mass from the combined $\sigma_{t\bar{t}}$ and have found the result to be consistent with the world average top quark mass [6] from direct measurements.

We thank the staffs at Fermilab and collaborating institutions, and acknowledge support from the DOE and NSF (USA); CEA and CNRS/IN2P3 (France); FASI, Rosatom and RFBR (Russia); CNPq, FAPERJ, FAPESP and FUNDUNESP (Brazil); DAE and DST (India); Colciencias (Colombia); CONACyT (Mexico); KRF and KOSEF (Korea); CONICET and UBACyT (Argentina); FOM (The Netherlands); STFC and the Royal Society (United Kingdom); MSMT and GACR (Czech Republic); CRC Program, CFI, NSERC and WestGrid Project (Canada); BMBF and DFG (Germany); SFI (Ireland); The Swedish Research Council (Sweden); CAS and CNSF (China); and the Alexander von Humboldt Foundation (Germany).

[a] Visitor from Augustana College, Sioux Falls, SD, USA.
[b] Visitor from Rutgers University, Piscataway, NJ, USA.
[c] Visitor from The University of Liverpool, Liverpool, UK.
[d] Visitor from Centro de Investigacion en Computacion - IPN, Mexico City, Mexico.
[e] Visitor from ECFM, Universidad Autonoma de Sinaloa, Culiacán, Mexico.
[f] Visitor from Helsinki Institute of Physics, Helsinki, Finland.
[g] Visitor from Universität Bern, Bern, Switzerland.

[h] Visitor from Universität Zürich, Zürich, Switzerland.
[‡] Deceased.

[1] P. M. Nadolsky *et al.*, Phys. Rev. D **78**, 013004 (2008); W. Beenakker *et al.*, Phys. Rev. D **40**, 54 (1989).
[2] M. Cacciari *et al.*, JHEP **09**, 127 (2008); M. Cacciari, private communications.
[3] S. Moch and P. Uwer, Phys. Rev. D **78**, 034003 (2008); S. Moch and P. Uwer, private communications.
[4] N. Kidonakis and R. Vogt, Phys. Rev. D **78**, 074005 (2008); N. Kidonakis, private communications.
[5] J. Guasch, R. A. Jimenez and J. Sola, Phys. Lett. B **360**, 47 (1995).
[6] C. Amsler *et al.* [Particle Data Group], Phys. Lett. B **667**, 1 (2008).
[7] V. M. Abazov *et al.* [D0 Collaboration], submitted to Phys. Lett. B., arXiv:0901.2137 [hep-ex] (2009).
[8] V. M. Abazov *et al.* [D0 Collaboration], Phys. Rev. Lett. **100**, 192004 (2008).
[9] V. M. Abazov *et al.* [D0 Collaboration], Phys. Rev. D **76**, 092007 (2007).
[10] V. M. Abazov *et al.* [D0 Collaboration], Phys. Rev. D **76**, 052006 (2007).
[11] T. Scanlon, Ph.D. thesis, FERMILAB-THESIS-2006-43 (2006).
[12] V. M. Abazov *et al.* [D0 Collaboration], Phys. Rev. D **74**, 112004 (2006).
[13] T. Sjöstrand *et al.*, Comput. Phys. Commun. **135**, 238 (2001).
[14] G. Feldman and R. Cousins, Phys. Rev. D **57**, 3873 (1998).
[15] A. H. Hoang and I. W. Stewart, Nucl. Phys. Proc. Suppl. **185**, 220 (2008).
[16] We obtain $a = 6.82350 \times 10^9, b = 1.10480 \times 10^8, c = 8.80552 \times 10^5$ and $d = -1.767 \times 10^3$ for Eq. 4.